# Direct measurement of charge transfer in thermoelectric $Ca_3Co_4O_9$

G. Yang,[1] Q. Ramasse,[2] and R. F. Klie[1]
[1]*Department of Physics, University of Illinois at Chicago, Chicago, Illinois 60607, USA*
[2]*National Center for Electron Microscopy, Lawrence Berkeley National Laboratory, Berkeley, California 94720, USA*
(Received 30 July 2008; revised manuscript received 14 September 2008; published 27 October 2008)

The misfit-layered cobalt oxide $Ca_3Co_4O_9$ exhibits outstanding physical properties including high thermoelectric power, low thermal conductivity, low resistivity, and high thermal stability. We utilize atomic-resolution *Z*-contrast imaging in conjunction with electron energy-loss spectroscopy (EELS) in an aberration-corrected scanning transmission electron microscope (STEM) to characterize the local atomic and electronic structure of $Ca_3Co_4O_9$. We will show that the position of the O atoms in the $CoO_2$ layers can be directly imaged, and that the CoO columns in the rocksalt layer exhibit a strong modulation in the (010) direction. Further, we measure the local Co valence and find significant hole transfer from the rocksalt CoO to the hexagonal $CoO_2$ layers. Our results are confirmed by self-consistent multiple-scattering calculations and we conclude that this hole transfer increases the mobile hole concentration and breaks the electron-hole symmetry in the $CoO_2$ layers, thereby enabling the high thermoelectric power in the strongly correlated $CoO_2$ subsystem.

DOI: 10.1103/PhysRevB.78.153109 PACS number(s): 72.15.Jf, 68.37.Ma, 79.20.Uv

Layered cobaltate materials have been the focus of many recent studies due to the wide variety of electrical, magnetic, and structural properties they exhibit. One of these properties is the two-dimensional superconductivity found in water-intercalated $Na_xCoO_2$,[1] where the superconducting $CoO_2$ sheets are separated by insulating layers of Na ions. While the structural similarities between $Na_xCoO_2$ and the high-$T_c$ superconducting (HTS) copper oxides such as $YBa_2Cu_3O_7$ are striking, the superconducting mechanism of $Na_xCoO_2$ appears more similar to $Sr_2RuO_4$, where a superconducting triplet state is found due to triangular lattice symmetry of the $CoO_2$ layer.[2] Another outstanding property of layered cobaltates is the large thermoelectric power in materials such as $NaCo_2O_4$,[3] $(CaOH)_{1.14}$ $CoO_2$,[4,5] $Ca_3Co_4O_9$,[6] and $(Bi_2Sr_2O_4)_x$ $CoO_2$.[7] The crystal structure of all these materials is very similar, with a $CdI_2$-typed conducting $CoO_2$ layer that is separated by an insulating rocksalt-typed structure with *n* layers, where $n=1$ for $NaCo_2O_4$, $n=2$ for $(CaOH)_{1.14}$ $CoO_2$, and so on. These layered structures exhibit a low electric resistivity $\rho$ and thermal conductivity $\kappa$, resulting in a figure of merit $ZT$ ($ZT=\frac{S^2T}{\rho\kappa}$) comparable to that of traditional intermetallic thermoelectric materials such as $Bi_2Te_3$ and $CoSb_3$ while exhibiting superior thermal stability.

Since its discovery in 1997,[3] the high thermoelectric power in $NaCo_2O_4$ has been attributed to a number of different mechanisms, including the large effective mass of the charge carriers due to the strong correlations in the $CoO_2$ subsystem, the spin degree freedom of charge carriers, and the occurrence of a mixed-valence state in the $CoO_2$ layer or a pseudogap. Similar mechanisms have also been suggested for the other layered thermoelectric cobalt oxide materials. It is interesting to note here that the structure of the $CoO_2$ layer remains nearly unchanged[8] while the thermoelectric power of the different layered cobaltate compounds increases as the thickness of the insulating rocksalt layer increases from 100 $\mu$V/K at 300 K in $L_2$ (Ref. 3) to 140 $\mu$V/K at 300 K in Pb and Ca doped $(Bi_2Sr_2O_4)_x$ $CoO_2$.[7] Therefore, the insulating rocksalt layer must play a crucial role in the high thermoelectric power of these misfit-layered compounds.

Among the different layered cobaltate systems, the $Ca_3Co_4O_9$ stands out as the only system containing one cation with nominally different oxidation states, namely $Co^{2+}$ in the rocksalt buffer layers ($Ca_2CoO_3$) and $Co^{4+}$ in the octahedral $CoO_2$ layers, which makes it an ideal system for studying effects such as charge transfer, orbital ordering, and spin-state transitions on the material's thermoelectric behavior. The structure of $Ca_3Co_4O_9$ has been reported to be monoclinic with two misfit layered subsystems, a distorted rocksalt-type $Ca_2CoO_3$ layer sandwiched between two $CdI_2$-typed $CoO_2$ layers along the *c* axis. Both subsystems share the same lattice parameters with $a=4.8339$ Å, $c=10.8436$ Å, and $\beta=98.14°$, but along the *b* axis the incommensurate structure results in $b_1=2.8238$ Å for the $CoO_2$ subsystem and $b_2=4.5582$ Å for the $Ca_2CoO_3$ subsystem.[9] The triangular $CoO_2$ layer consists of edge sharing oxygen octahedra, and recent studies have shown that $CoO_2$ is a metal near a Mott transition with a unit-cell parameters of $a=b=2.806$ Å.[10] Therefore, the $CoO_2$ subsystem in $Ca_3Co_4O_9$ is subject to compressive strain in the *a*-axis direction, and several studies have shown that increasing the compressive strain will further increase the thermoelectric power.[11–13]

It has also been suggested that the occurrence of a mixed Co valence state in the $CoO_2$ layers and the transition of different Co-ion spin states play a crucial role in understanding the high thermoelectric properties of $Ca_3Co_4O_9$. Previous studies on Co valences estimated the Co valence to be +3.5 in the $CoO_2$ layers and +2.8 in CoO layers based on the measured average bond length.[14] Moreover, previous powder x-ray and neutron-diffraction experiments have suggested a strong undulation of O atomic sites in the $CoO_2$ layers and a strong displacive modulation of both the Co and O sites in the rocksalt subsystem.[9,15] However, due to the complex structure of this incommensurate, layered system, and the resulting large unit-cell, no detailed atomic-resolution studies of the local atomic and electronic structures have been reported to date.

In this Brief Report, we present an atomic-resolution study of $Ca_3Co_4O_9$ using aberration-corrected *Z*-contrast

 

imaging[16] and atomic-column resolved electron energy-loss spectroscopy (EELS) (Ref. 17) in combination with *ab initio* real-space multiple-scattering (MS) calculations[18] of the energy-loss near-edge structure (ELNES). The $Ca_3Co_4O_9$ samples were prepared from high-purity $CaCO_3$ and $Co_3O_4$ powders that were mixed stoichiometrically and then calcined at 880 °C for 24 h in flowing air. Previous $Ca_3Co_4O_9$ samples that were prepared using similar methods did not show any significant concentration of O or Co vacancies.[6] Further, elemental analysis using energy dispersive (EDS) x-ray analysis does not show any significant variation in the Ca or Co concentration within the $Ca_3Co_4O_9$ sample, in contrast to a prior study.[19] Thus, we assume the sample to be stoichiometric $Ca_3Co_4O_9$. The atomic-resolution STEM images and EELS spectra were obtained using an aberration corrected VG HB 501 dedicated STEM (Ref. 20) and the TEAM instrument (FEI Titan 300 kV TEM/STEM) located at the National Center for Electron Microscopy (NCEM). Particular attention was paid to the effects of electron irradiation on the sample materials to assure that all the results reported here are not attributable to electron-beam damage. The self-consistent *ab initio* multiple-scattering calculations were performed using the FEFF8.4 code[18] using a real-space structure of $Ca_3Co_4O_9$ containing about 100 atoms. The incommensurate structure of $Ca_3Co_4O_9$ was reproduced by alternating the stacking of rocksalt $Ca_2CoO_3$ subsystems with $b_2$=4.5582 Å and $CoO_2$ subsystems with $b_1$=2.8238 Å along the $c$ axis.

Figure 1(a) shows an atomic-resolution $Z$-contrast image of $Ca_3Co_4O_9$ (acquired using the FEI Titan) in the [010] orientation, clearly exhibiting the four distinct layers of varying brightness. The $CoO_2$ layer can be seen as the brightest layer followed by the CaO, CoO, and CaO layer, respectively. The incommensurate structure of $Ca_3Co_4O_9$ is not visible in this orientation as indicated in the structural model shown in Fig. 1(a). Atomic-resolution $Z$-contrast images obtained in the [100] orientation (not shown here) clearly reveal the misfit-layered structure.[21] It is interesting to note here that while the atomic columns in the $CoO_2$ and CaO layers can be clearly resolved, the atomic columns in the CoO layers appear blurred. This is not due to insufficient spatial resolution. On the contrary, in the $CoO_2$ layers not only can the Co atomic columns be seen, but even the O atomic columns are resolved as detailed later. The electron probe size is calculated to be about 0.8 Å using Haider's d59 criterion[22] [or close to a full width at half maximum (FWHM) of 0.5 Å]. Figure 1(b) shows an intensity profile taken across a Co and O atomic columns in the $CoO_2$ layer. Here, the Co columns are shown as the brightest intensity peak, while the shoulders on both sides correspond to the relative intensities expected for O using a $Z^2$ intensity argument. Moreover, the positions of the O columns correspond to those in our $Z$-contrast image simulations [Fig. 1(c)]. The direct visualization of O atomic columns using $Z$-contrast imaging has so far been reported only in very few special cases[23] and requires that the atomic O site are highly ordered along the electron-beam direction, since the scattering amplitude of O at high scattering angles is low compared to elements such as Ca, Ti, or Co. $Z$-contrast image simulations [Fig. 1(c)] of $Ca_3Co_4O_9$ further confirm that the CoO columns should be clearly resolved in the undistorted $Ca_3Co_4O_9$ structure. Therefore, our ability to resolve the O columns in the $CoO_2$ layers and not the Co in the rocksalt layers leads the conclusion that contrary to prior reports,[9] the O atomic sites in the $CoO_2$ layers do not exhibit any displacive modulation, while the Co and O sites in the $Ca_2CoO_3$ layers ex-

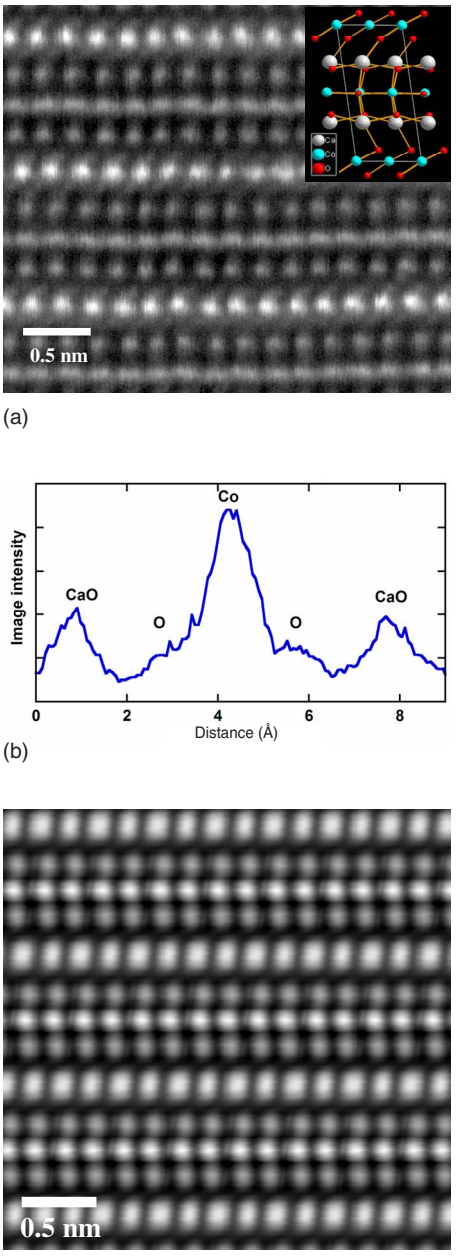


FIG. 1. (Color online) (a) Atomic resolution $Z$-contrast image of $Ca_3Co_4O_9$ in the [010] orientation. The brightest atomic columns show the Co atoms in the $CoO_2$-layer with the adjacent O atoms clearly visible. The inset shows a model of the $Ca_3Co_4O_9$ unit-cell in the same orientation. (b) Line scan of the image intensity across a Co atomic column and two adjacent O columns. The O columns can be clearly seen as distinct peaks next to the Co column. (c) Calculated $Z$-contrast image of $Ca_3Co_4O_9$ [010] showing that the CoO column in the middle of the rocksalt $Ca_2CoO_3$ should be resolved clearly in the experimental image.

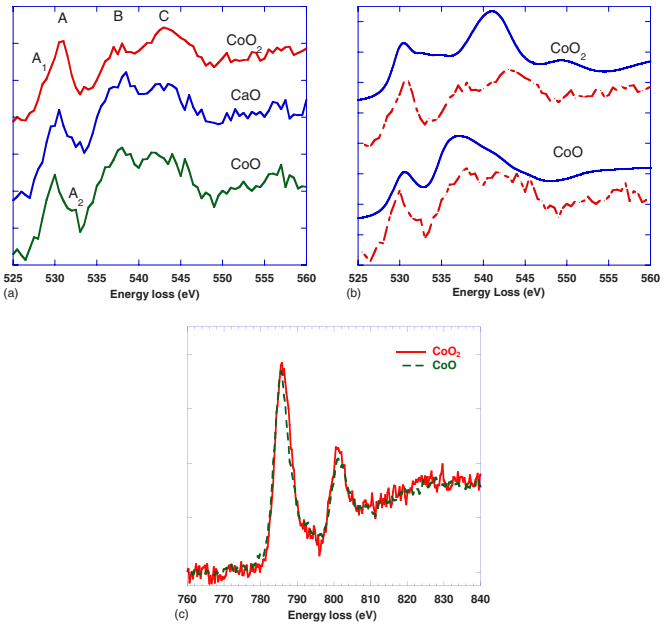


FIG. 2. (Color online) (a) Oxygen *K*-edge spectra of different layers in $Ca_3Co_4O_9$, the energy scale is calibrated to the Ca $L_3$-edge onset, while the intensity is normalized to the prepeak A intensity; (b) calculated O *K*-edge spectra for the different Co-O layers using the multiple-scattering code FEFF8.4 (solid line) and experimental spectra (as shown in a), dotted line. (c) Co *L* edges for the different Co-O layers showing the Co $L_3$ and the $L_2$ white lines. The spectra are normalized to the Co $L_3$ peak intensity. All experimental spectra are averaged over three individual spectra.

hibit a large undulation along the *b* axis. A recent XRD study of single-crystal $Ca_3Co_4O_9$ reports the existence of occupational modulation in the CoO layer resulting in triple chains along the *b* direction.[15]

Atomic-column resolved electron energy-loss spectra (acquired using the VG HB 501) of the different layers in the $Ca_3Co_4O_9$ unit cell are shown in Fig. 2. Figure 2(a) shows the O *K*-edge spectrum acquired from the $CoO_2$, the CaO, and the CoO layers. The near-edge fine structure of the O *K*-edge spectra can be divided into two regions, the prepeak from ~526 to ~533 eV and the main peak from ~533 to ~549 eV. The prepeak region contains a dominant peak at 530 eV (labeled A) and a small satellite peak at 528.5 eV (labeled $A_1$) in $CoO_2$ spectrum and 532.5 eV (labeled $A_2$) in CoO spectrum. By comparing the experimental spectra from the $CoO_2$ and the CoO layers with EELS spectra from similar materials, such as $LaCoO_3$ (Ref. 24 and 25) and the results of our MS calculations, we find that peak A stems from transitions from the O 1*s* into the hybridized O 2*p*-Co 3*d* orbitals.[26] In this layered cobaltate material the Co $t_{2g}$ states are further split into $a_{1g}$ and $e_{g'}$ orbital due to the rhombohedral distortion of the $CoO_2$ layer, with the $a_{1g}$ orbital at a higher energy than the $e_{g'}$.[27,28] Therefore, peak $A_1$ in the $CoO_2$ spectrum stems from the transitions to hybridized O 2*p* and $Co^{4+}$ $a_{1g}$ states, while no such peak is observed in CoO spectrum. The peak $A_2$ in the CoO spectrum is characteristic of a $Co^{3+}$ oxidation state due to transitions to hybridized O 2*p*-$Co^{3+}$ $e_g$ states,[29] which indicates the presence of $Co^{3+}$ ions in CoO layers. Finally, the first peak of the main O *K*-edge (peak B) has been shown to originate from transitions to hybridized O 2*p*-Ca 4*sp* orbitals,[30,31] while peak C has been attributed to the transitions to the hybridized O 2*p*-Co 4*sp* band. Therefore, the high intensity of peak C in the $CoO_2$ and CoO spectra indicates strong Co-O bonding, while the high intensity of peak B in the CaO and CoO spectra shows high Ca-O bonding.

Figure 2(b) shows the results of our *ab initio* multiple-scattering calculations of oxygen *K*-edge near-edge fine structure for the CoO and the $CoO_2$ spectra. The calculated spectra take into consideration only the contribution from the Co-O atomic columns and the effects of beam dechanneling have not been accounted for. Thus, the calculated spectrum for the $CoO_2$ layer shows only the prepeak A and the peak C, while the spectrum for the CoO layer shows the prepeak A and the peak B. Note that the energy scale of the calculated spectra has not been altered, and that the model used in the calculations assumes the stoichiometric CoO and $CoO_2$, respectively. It can be seen from Fig. 2(b) that the intensity of peak A relative to the main peak is slightly higher for the $CoO_2$ spectrum compared to CoO. This difference can be explained by the different occupancy of the Co orbitals assuming the ideal valence state of $Co^{4+}$ and $Co^{2+}$, respectively. However, in the experimental spectra, the intensity of peak A is substantially higher in $CoO_2$ compared to that of the calculated $CoO_2$ spectrum. It has been previously shown that the prepeak can be used to quantify the density of hole states.[32,33] Therefore, the higher prepeak in $CoO_2$ layers indicates a higher concentration of mobile holes, which could explain the two-dimensional *p*-type thermoelectric behavior of the $CoO_2$ layers.

Figure 2(c) shows the Co *L* edge from the $CoO_2$ and the CoO, respectively. By using the relationship between the Co $L_3$, $L_2$ white lines and the Co valence reported by Wang *et al.*,[34] we find that a mixed-valence state exists in the $CoO_2$ layers with a nominal Co valence of 3.5+, while the valence in the CoO layers is 3.0+. This measured Co valence state is in good agreement with previous estimates. However, compared to the expected valence state of Co for charge neutral CoO and $CoO_2$ layers, we find the CoO layer in the rocksalt $Ca_2CoO_3$ layer to be positively charged $[(CoO)^{1+}]$, while the hexagonal $CoO_2$ layer is negatively charged $[(CoO_2)^{0.5-}]$. By preserving the overall charge neutrality of both layers, holes are now transferred from the CoO to the $CoO_2$ layer, resulting in the high concentration of mobile holes measured in the $CoO_2$ layer. It has been previously shown that such a hole transfer is essential for the thermoelectric effect since it not only provides the necessary mobile charge carriers, but the existence of a half-filled band (or the existence of particle-hole symmetry) as in the case for $Co^{4+}$ in the $CoO_2$ layers, will result in a zero thermoelectric power (Seebeck coefficient).[35] The observed hole transfer will thus remove the orbital degeneracy [$t_{2g}$ split into a $a_{1g}$ and $e_{g'}$ orbitals, as observed in Fig. 2(a)], thereby explaining the nonzero thermopower in $Ca_3Co_4O_9$. Finally, we did not find any signs of charge or orbital ordering occurring in the $CoO_2$ layers that had been previously suggested to be responsible for the high thermoelectric power in $Ca_3Co_4O_9$.

In summary, we find that the atomic structure of $Ca_3Co_4O_9$ is made of compressed $CoO_2$ layers that do not

exhibit substantial modulations of either the Co or O atomic positions and a triple rocksalt layer ($Ca_2CoO_3$) with strong buckling of the CoO layer along the *b* axis. We have shown that using aberration-corrected *Z*-contrast imaging, the O atomic sites can be directly imaged in the $CoO_2$ layer, confirming that the O atoms are not significantly displaced along the *b* direction. We have further shown that the two different kinds of Co sites that exist in $Ca_3Co_4O_9$ play completely different roles in its thermoelectric behavior, namely to provide charge carriers to the $CoO_2$ layer and to conduct holes along the $CoO_2$ layer. Our results, in particular the hole transfer from the rocksalt subsystem to the $CoO_2$ layer and the increase in the mobile hole-state concentration in the $CoO_2$ layer, suggest that the hole doping of the $CoO_2$ layers results in an increased density of mobile hole states, which is essential in breaking the particle-hole symmetry of the half-filled Co-band thereby allowing a nonzero thermoelectric power. Our results further show that the transport properties of the $CoO_2$ layers are governed by itinerant holes.

In conclusion, we have shown that the hole transfer, which occurs of a over a distance of at least 5 Å in $Ca_3Co_4O_9$ plays a crucial role in understanding the atomic-scale mechanisms that govern the high thermoelectric properties in these misfit layered materials. Future experiments will have to clarify the role of interfacial strain and Co-ion spin-state transitions on the hole transfer, and explore the optimum thickness of the rocksalt reservoir layer. Further, the structural and charge transfer models reported here will provide an important piece to the puzzle of two-dimensional superconductivity found in water-intercalated $Na_x$ $CoO_2$.

We thank Q. Li of Brookhaven National Laboratory for the sample synthesis. The work at the National Center for Electron Microscopy is supported by the U. S. Department of Energy under Contract No. DE-AC02-05CH11231.

[1] K. Takada, H. Sakurai, E. Takayama-Muromachi, F. Izumi, R. A. Dilanian, and T. Sasaki, Nature (London) **422**, 53 (2003).
[2] D. J. Singh, Phys. Rev. B **68**, 020503(R) (2003).
[3] I. Terasaki, Y. Sasago, and K. Uchinokura, Phys. Rev. B **56**, R12685 (1997).
[4] M. Shizuya, M. Isobe, Y. Baba, T. Nagai, M. Osada, K. Kosuda, S. Takenouchi, Y. Matsui, and E. Takayama-Muromachi, J. Solid State Chem. **180**, 249 (2007).
[5] M. Isobe, M. Shizuya, and E. Takayama-Muromachi, J. Magn. Magn. Mater. **310**, E269 (2007).
[6] A. C. Masset, C. Michel, A. Maignan, M. Hervieu, O. Toulemonde, F. Studer, B. Raveau, and J. Hejtmanek, Phys. Rev. B **62**, 166 (2000).
[7] R. Funahashi and I. Matsubara, Appl. Phys. Lett. **79**, 362 (2001).
[8] D. Grebille, H. Muguerra, O. Perez, E. Guilmeau, H. Rousseliere, and R. Funahashi, Acta Crystallogr., Sect. B: Struct. Sci. **63**, 373 (2007).
[9] Y. Miyazaki, M. Onoda, T. Oku, M. Kikuchi, Y. Ishii, Y. Ono, Y. Morii, and T. Kajitani, J. Phys. Soc. Jpn. **71**, 491 (2002).
[10] C. de Vaulx, M. H. Julien, C. Berthier, S. Hebert, V. Pralong, and A. Maignan, Phys. Rev. Lett. **98**, 246402 (2007).
[11] I. Matsubara, R. Funahashi, M. Shikano, K. Sasaki, and H. Enomoto, Appl. Phys. Lett. **80**, 4729 (2002).
[12] G. J. Xu, Appl. Phys. Lett. **80**, 3760 (2002).
[13] Y. F. Hu, W. D. Si, E. Sutter, and Q. Li, Appl. Phys. Lett. **86**, 082103 (2005).
[14] S. Lambert, H. Leligny, and D. Grebille, J. Solid State Chem. **160**, 322 (2001).
[15] H. Muguerra, D. Grebille, and F. Bouree, Acta Crystallogr., Sect. B: Struct. Sci. **64**, 144 (2008).
[16] S. J. Pennycook and L. A. Boatner, Nature (London) **336**, 565 (1988).
[17] R. Egerton, *Electron Energy Loss Spectroscopy in the Electron Microscope*, 2nd ed. (Plenum, New York, 1996).
[18] A. L. Ankudinov, B. Ravel, J. J. Rehr, and S. D. Conradson, Phys. Rev. B **58**, 7565 (1998).
[19] M. Karppinen, H. Fjellvag, T. Konna, Y. Morita, T. Motohashi, and H. Yamauchi, Chem. Mater. **16**, 2790 (2004).
[20] M. Varela, A. R. Lupini, K. van Benthem, A. Y. Borisevich, M. F. Chisholm, N. Shibata, E. Abe, and S. J. Pennycook, Annu. Rev. Mater. Res. **35**, 539 (2005).
[21] R. F. Klie (unpublished).
[22] M. Haider, S. Uhlemann, and J. Zach, Ultramicroscopy **81**, 163 (2000).
[23] M. F. Chisholm, A. R. Lupini, S. J. Pennycook, I. Ohkubo, H. M. Christen, S. D. Findlay, M. Oxley, and L. J. Allen, Microsc. Microanal. **10**, 256 (2004).
[24] F. M. F. de Groot, M. Abbate, J. Vanelp, G. A. Sawatzky, Y. J. Ma, C. T. Chen, and F. Sette, J. Phys.: Condens. Matter **5**, 2277 (1993).
[25] R. F. Klie, J. C. Zheng, Y. Zhu, M. Varela, J. Wu, and C. Leighton, Phys. Rev. Lett. **99**, 047203 (2007).
[26] F. M. F. de Groot, M. Grioni, J. C. Fuggle, J. Ghijsen, G. A. Sawatzky, and H. Petersen, Phys. Rev. B **40**, 5715 (1989).
[27] D. J. Singh, Phys. Rev. B **61**, 13397 (2000).
[28] W. B. Wu, D. J. Huang, J. Okamoto, A. Tanaka, H. J. Lin, F. C. Chou, A. Fujimori, and C. T. Chen, Phys. Rev. Lett. **94**, 146402 (2005).
[29] M. Valkeapaa, Y. Katsumata, I. Asako, T. Motohashi, T. S. Chan, R. S. Liu, J. M. Chen, H. Yamauchi, and M. Karppinen, J. Solid State Chem. **180**, 1608 (2007).
[30] H. O. Moltaji, J. P. Buban, J. A. Zaborac, and N. D. Browning, Micron **31**, 381 (2000).
[31] H. Gu and M. Ceh, Ultramicroscopy **78**, 221 (1999).
[32] A. R. Moodenbaugh, B. Nielsen, S. Sambasivan, D. A. Fischer, T. Friessnegg, S. Aggarwal, R. Ramesh, and R. L. Pfeffer, Phys. Rev. B **61**, 5666 (2000).
[33] N. D. Browning, M. F. Chisholm, S. J. Pennycook, D. P. Norton, and D. H. Lowndes, Physica C **212**, 185 (1993).
[34] Z. L. Wang, J. Bentley, and N. D. Evans, Micron **31**, 355 (2000).
[35] G. Beni and C. F. Coll, Phys. Rev. B **11**, 573 (1975).